Research Article | Vol. 27, No. 23 / 11 November 2019 / Optics Express 33745

Optics EXPRESS

M-QAM transmission over hybrid microwave photonic links at the K-band

DONG-NHAT NGUYEN,[1,*] JAN BOHATA,[1] JAN SPACIL,[1] DANIEL DOUSEK,[1] MATEJ KOMANEC,[1] STANISLAV ZVANOVEC,[1] ZABIH GHASSEMLOOY,[2] AND BEATRIZ ORTEGA[3]

[1]*Department of Electromagnetic Field, Faculty of Electrical Engineering, Czech Technical University in Prague, Prague 166 27, Czech Republic*
[2]*Optical Communication Research Group, Northumbria University, Newcastle upon Tyne NE1 8ST, UK*
[3]*Instituto de Telecomunicaciones y Aplicaciones Multimedia, ITEAM, Universitat Politècnica de València, Camino de Vera, Valencia 46022, Spain*
[*]*dongnhat@fel.cvut.cz*

Abstract: Two experimental configurations of a hybrid K-band (25 GHz) microwave photonic link (MPL) are investigated for seamless broadband wireless access networks. Experimental configurations consist of optical fiber, free-space optics (FSO) and radio frequency (RF) wireless channels. We analyze in detail the effects of channel impairments, namely fiber chromatic dispersion, atmospheric turbulence and multipath-induced fading on the transmission performance. In the first configuration, transmission of the 64-quadrature amplitude modulation (QAM) signal with 5, 20 and 50 MHz bandwidths over 5 km standard single-mode fiber (SSMF), 2 m turbulent FSO and 3 m RF wireless channels is investigated. We show that, for QAM with a high bandwidth, the link performance is being affected more by atmospheric turbulence. In the second configuration, the 20 MHz 4/16/64-QAM signals over a 50 km SSMF and 40 m FSO/RF wireless links are successfully transmitted with the measured error vector magnitude (EVM) values of 12, 9 and 7.9%, respectively. It is shown that, for all transmitted microwave vector signals, the bit error rate is lower than the hard-decision forward-error-correction limit of 3.8×10^{-3}. Moreover, an extended FSO link span of 500 m for 25 GHz hybrid MPL with 16-QAM at 10 Gb/s under the weak and strong turbulence regimes is evaluated via simulation analysis to mimic a practical outdoor system.

1. Introduction

The low-frequency range (< 6 GHz) in the radio frequency (RF) spectrum adopted for broadband wireless access (BWA) networks is overloaded due to the growing use of wireless technologies in recent years [1–3]. In order to increase the network capacity and efficiency as well as offer the users certain unique benefits, the next-generation BWA networks should operate at higher-carrier frequencies i.e., millimeter-wave (MMW) bands. The radio-over-fiber (RoF) or microwave photonic link (MPL) technology operating at the MMW band has recently been investigated as a viable solution for high-capacity networks (i.e., up to 24 Gb/s per lambda) [4–7]. In centralized architectures, these systems use optical fibers (OFs) as the transmission medium to transfer data from the central office to the base stations, where the MMW signal is wirelessly transmitted to the end users. However, in practical OF-based MPLs there are several drawbacks including (i) installation time; (ii) right of access to public spaces; and (iii) natural disasters [8]. Recent literature reports a number of MPL schemes with an extended fiber-reach, e.g., 4- and 16-quadrature amplitude modulated (QAM) signals at 2.5 GHz were successfully transmitted over a 25 km of standard single-mode fiber (SSMF) using a coherent receiver and advanced digital signal processing for phase noise cancellation [1]. A 6 GHz link transmitting 4- and 16-QAM was also demonstrated over a 25 km of SSMF with optimization of the chromatic dispersion

#376377 https://doi.org/10.1364/OE.27.033745
Journal © 2019 Received 27 Aug 2019; revised 22 Oct 2019; accepted 22 Oct 2019; published 4 Nov 2019

Optics EXPRESS

induced power fading [3]. Note that, RF wireless transmission was not considered in these works and therefore multipath-induced fading has not been investigated. An attractive alternative wireless transmission option in MPLs is the free-space optics (FSO) technology, which offers similar capabilities as OFs, i.e., huge bandwidth, electromagnetic immunity and wavelength division multiplexing (WDM) compatibility with significantly reduced deployment costs [8,9]. The concept of radio over FSO, denoted as RoFSO, has been introduced and standardized by International Telecommunication Union [10]. Since then, further experimental demonstrations have been reported in this field. In 2012, orthogonal frequency-division-multiplexing (OFDM)-based digital television signals were successfully transmitted over a 1 km FSO link under different outdoor weather conditions [11]. In 2016, 4 Gb/s 16-QAM-OFDM signal at 60 GHz was transmitted over 1.83 m FSO and RF wireless links and evaluated with synthesized weather conditions i.e., fog, rain and turbulence [12]. In 2018, we demonstrated 100 MHz 64-QAM transmission at different carrier frequencies of 24–26 GHz using a low-cost directly modulated laser over 2 m turbulent FSO and 3.6 m RF wireless links with the lowest measured EVM of 4.7% [13]. Very recently, the transmission of 1 Gbaud 16-QAM at 28 GHz over a 0.9 m FSO channel with dust and a 1 m RF wireless link was demonstrated with a bit error rate (BER) well below the hard-decision forward-error-correction (HD-FEC) limit of 3.8×10^{-3} [14].

In recent years only a limited number of works on RoFSO systems operating at MMW carrier frequency have been reported in the literature as outlined in Table 1. Therefore, it is timely to report on a RoFSO system utilizing the K-band (i.e., 25 GHz) QAM signals over a 40-meter-long FSO channel, which is so far the longest reported FSO transmission of such signals. Note that, the 25 GHz carrier frequency is optically generated by frequency multiplication with the optical carrier suppression (OCS) scheme using an optical modulator. This MMW band has gained increasing attention in recent years as part of the 5th generation (5G) wireless networks [15,16]. In addition, the photonic up-conversion-based technique has been investigated by both the research community and the commercial sector in the past several years [17–19]. This is because the OCS offers significant advantages such as (i) relaxed requirements on RF components; (ii) higher tolerance to chromatic dispersion; (iii) wavelength reuse for the uplink; and (iv) lower phase noise due to the fact that the two sidebands are produced by the same laser.

Table 1. Summary of recent RoFSO transmission experiments with MMW carrier frequencies from 2016–2019

Modulation format	Bit rate	Carrier frequency (frequency band)	FSO distance (m)	Year	Reference
16-QAM	4 Gb/s	60 GHz (V)	1.83	2016	[12]
64-QAM	600 Mb/s	24–26 GHz (K)	2	2018	[13]
4/16-QAM	6/12 Gb/s	25 GHz (K)	8	2018	[20]
16-QAM	4 Gb/s	28 GHz (K_a)	0.9	2019	[14]
4/16/64-QAM	40/80/120 Mb/s	60 GHz (V)	1	2019	[21]
64-QAM	18/75/300 Mb/s	25 GHz (K)	2	2019	**This work**
4/16/64-QAM	16/31/75 Mb/s	25 GHz (K)	40	2019	**This work**

In specific, we demonstrate a proof-of-concept seamless hybrid MPL scheme composed of RoF, RoFSO and RF wireless transmission for two configurations. In configuration A, we focus on the effect of atmospheric turbulence-induced fading on 64-QAM with a variable bandwidth transmitted over the proposed hybrid MPL consisting of 5 km SSMF, 2 m turbulent FSO and 3 m RF wireless channels. In configuration B, M-QAMs for $M = 4$, 16 and 64 with the bandwidth of 20 MHz are transmitted over the proposed hybrid MPL consisting of SSMF (5 or 50 km) and FSO/RF indoor wireless links (40 m each). The multipath-induced fading in RF wireless channel is examined.

Optics EXPRESS

The remainder of the paper is organized as follows. Section 2 describes the two experimental configurations and the supporting theoretical basis for turbulence characterization. Section 3 presents and discusses the corresponding experimental results. Section 4 presents the simulation analysis of the proposed hybrid MPL with a FSO link span extended up to 500 m under the weak and strong turbulence regimes for practical outdoor applications. Finally, section 5 concludes the paper.

2. Experimental Setup of Hybrid MPL

2.1. Configuration A

Figure 1 shows the schematic diagram of the experimental setup for the hybrid MPL (configuration A). The insets (i) and (ii) show the laboratory testbed and the controlled FSO channel, respectively. At the transmitter (Tx), a continuous wave optical signal emitted by the laser (ID Photonics CoBrite-DX4) was applied through a polarization controller (PC) into a single-drive Mach-Zehnder modulator (MZM 1) where it is externally modulated by a 12.5 GHz RF clock signal generated by a signal generator (R&S SMF 100A) with an output power of 18 dBm. Note that, MZM 1 was biased at the minimum transmission point and therefore its output optical spectrum showed double-sideband with OCS having a frequency spacing of 25 GHz (i.e., twice the original RF clock signal frequency), see the inset (iv) in Fig. 1. The measured optical carrier to sideband ratio (CSR) was 27 dB at a bias voltage of 3.4 V and was adopted in all modulation formats for a fair comparison. Next, the output of MZM 1 was launched via another PC into MZM 2, which is externally modulated by a 64-QAM signal with an intermediate frequency (IF) of 200 MHz and output power of 4 dBm, generated by a vector signal generator (R&S SMW 200A). Note that, this output power is chosen following a number of tests that were carried out for different power levels ranging from -10 to 8 dBm. The selected value was based on the low EVM value and low nonlinear distortion. In this work, we have considered the bandwidth of 5, 20 and 50 MHz for the 64-QAM signal.

The up-converted signal was then applied to the WDM multiplexer (MUX) serving to mimic practical high-capacity multi-wavelength networks prior to being launched into a 5 km of SSMF. By using two doublet optical collimators (Thorlabs F810APC-1550), the light was launched from the SSMF into a free-space link and injected back into the SSMF at the receiver (Rx) side. An external fan heater was used to generate turbulence by blowing hot air perpendicularly to the propagating optical beam, see inset (ii) in Fig. 1. Note, we have used an atmospheric chamber with a dimension of 2 ×0.4 ×0.4 m^3 to mimic the turbulent FSO channel. For this purpose, 20 thermal sensors were equidistantly spaced (i.e., by 10 cm) along the chamber to accurately measure the thermal profiles.

The measured thermal profiles were then used to determine the refractive index structure parameter C_n^2 [$m^{-2/3}$], which defines the strength of turbulence, given as [22]:

$$C_n^2 = \left(79 \times 10^{-6} \frac{P}{T^2}\right)^2 C_T^2, \tag{1}$$

where P is atmospheric pressure in millibar, T is the absolute temperature in Kelvin and C_T^2 is the thermal structure parameter defined as:

$$C_T^2 = (T_1 - T_2)^2 / d^{2/3}, \tag{2}$$

where T_1 and T_2 are the temperatures measured at two adjacent thermal sensors separated by the propagation distance d (i.e., 10 cm). Note that, in this work the C_n^2 value was processed off-line with more than 1400 sets of thermal profiles. This is to maintain the same temperature profile along the chamber and ensure the fair comparison for all considered 64-QAM signals.

Optics EXPRESS

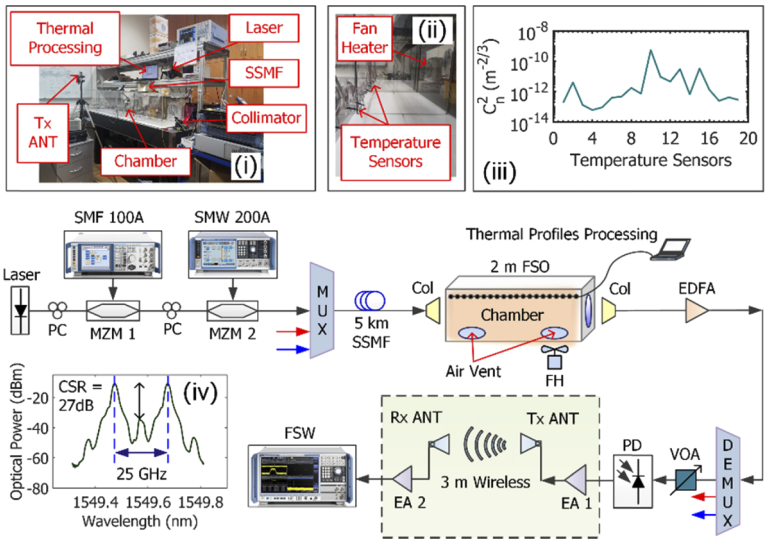

Fig. 1. Experimental configuration A. Insets: (i) Overview of the hybrid MPL setup, (ii) Turbulent FSO chamber, (iii) Recorded C_n^2 ($m^{-2/3}$) and (iv) Optical spectrum with a carrier-suppressed modulation scheme measured after MZM 1. PC: polarization controller, MZM: Mach-Zehnder modulator, MUX: multiplexer, Col: collimator, FH: fan heater, EDFA: erbium-doped fiber amplifier, DEMUX: de-multiplexer, VOA: variable optical attenuator, PD: PIN photodiode, EA: electrical amplifier and ANT: antenna.

The average C_n^2 values without and with turbulence using the laboratory FSO chamber are about 2.4×10^{-14} and 3.2×10^{-11} $m^{-2/3}$, respectively. Inset (iii) in Fig. 1 shows the recorded C_n^2 for the case of turbulence. Note, the high level of turbulence for the short-range indoor FSO link can be re-calculated based on Eq. (3) to determine the turbulence level for the longer range outdoor FSO link by retaining the same σ_R^2. Thus, C_n^2 of 3.2×10^{-11} $m^{-2/3}$ for a 2 m FSO link corresponds to the magnitudes of 1.3×10^{-15} and 3.6×10^{-16} $m^{-2/3}$ for the medium-distance FSO links of 500 and 1000 m, respectively. The measured FSO channel loss was 4 dB. Another important parameter that is commonly used to determine the turbulence strength is Rytov variance σ_R^2, given by [22]:

$$\sigma_R^2 = 1.23 C_n^2 k^{7/6} L^{11/6}, \tag{3}$$

where $k = 2\pi/\lambda$ is the optical wave number, λ is the laser wavelength and L is the FSO propagation distance (i.e., 2 m in this case). Note that, determining σ_R^2 is essential when scaling the FSO system performance from short-link indoor to long-distance outdoor environments.

The optical signal was amplified using an erbium-doped fiber amplifier (EDFA, Keopsys KPS-BT2-C-10-LN-SA,) with an output power of 3 dBm and applied to the wavelength demultiplexer (DEMUX) prior to direct detection using an InGaAs PIN photodiode (Optilab PD-40). The converted electrical signal was amplified using a low-noise electrical amplifier (EA 1, Miteq AMF-4F-260400-40-10p) with a gain and a noise figure of 27 and 2 dB, respectively. Afterward, the signal was transmitted over a 3 m RF wireless link using a pair of double-ridged waveguide horn antennas (ANT – RFSpin DRH40). The Tx and the Rx ANTs were identical with a gain of 15 dBi at the frequency of 25 GHz. Note, the ANTs were mounted on adjustable tripods in line of sight in order to maximize the signal strength at the Rx and reduce multipath-induced fading as well as to avoid the effect of the first Fresnel zone. At the Rx ANT output, the signal was further amplified using another low-noise EA 2 (Analog device HMC1131) with a gain and a noise figure of 22 and 1.7 dB, respectively. The signal was finally captured by a signal analyzer

Optics EXPRESS

(R&S FSW) for further assessment. The main system parameters adopted in the experiments are summarized in Table 2.

Table 2. Key experimental parameters

Parameter	Value (Configuration A)	Value (Configuration B)
Laser		
• Wavelength	1549.58 nm	1549.58 nm
• Output power	16 dBm	16 dBm
Data signal		
• Format	64-QAM	4/16/64-QAM
• Bandwidth	5/20/50 MHz	20 MHz
• Power	4 dBm	4 dBm
MMW carrier frequency	25 GHz	25 GHz
EDFA		
• Output power	3 dBm	7 dBm
• Noise figure	< 5 dB	< 5 dB
SSMF length (loss)	5 km (1dB)	5 and 50 km (1 and 10 dB)
FSO length (loss)	2 m (4 dB)	40 m (12 dB)
• Tx/Rx collimator aperture	24 mm	24 mm
PD		
• Responsivity	0.8 A/W @ 1550 nm	0.8 A/W @ 1550 nm
• Dark current	10 nA	10 nA
RF wireless length	3 m (40 dB)	40 m (62 dB)

2.2. Configuration B

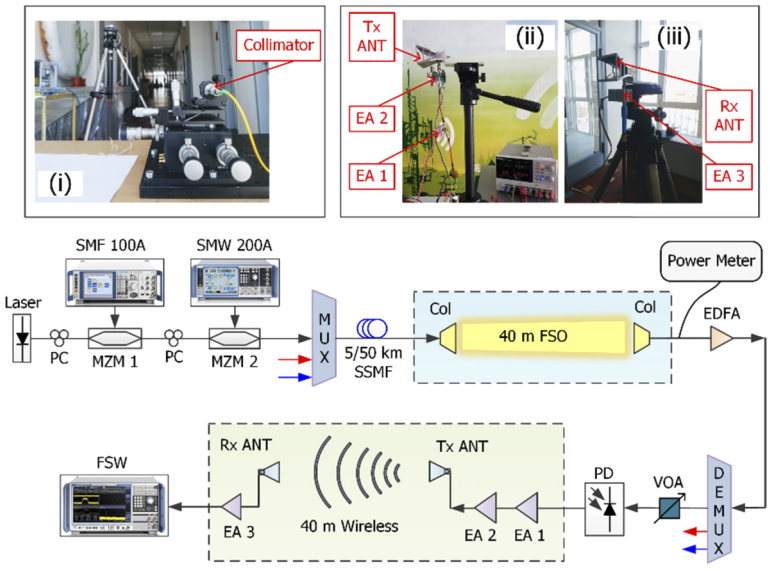

Fig. 2. Experimental configuration B. Insets: (i) FSO coupling, (ii) Tx ANT in the corridor and (iii) Rx ANT in the corridor.

Optics EXPRESS

The second set of experiments was carried out in a corridor of Faculty of Electrical Engineering, CTU in Prague with FSO and RF wireless channels extended up to 40 m as depicted in Fig. 2 (inset (i) and (ii)). Unlike configuration A, this testbed employed different modulation formats (i.e., 4/16/64-QAM) but using static signal bandwidth of 20 MHz. The SSMF link lengths were 5 and 50 km. At the output of the FSO channel, the optical power level was monitored by using a power meter connected to a 1% branch of a 1/99 coupler in order to ensure the FSO link alignment during the experiment. The measured FSO channel loss for 40 m was 12 dB. The EDFA output power was then set at 7 dBm and an additional EA 3 (Miteq AMF-4F-260400-40-10p) was used to boost the signal level. The remaining setup parameters were kept the same as in configuration A (see Table 2).

3. Experimental results and discussion

3.1. Configuration A

Figures 3(a) and (b) show the measured EVM as a function of received MMW power for the 64-QAM signal with 5, 20 and 50 MHz bandwidth following transmission over the hybrid MPL, which consists of SSMF (5 km), FSO (2 m) (without and with turbulence) and RF wireless channel (3 m). Also shown is the 8% EVM limit for 64-QAM, as defined in the third-generation partnership project (3GPP) specifications [23]. The EVM values were recorded over 90000 points and averaged over 50 sets of readings. Note that a variable optical attenuator (VOA) was used in front of the PD to adjust the level of received optical power and therefore the received MMW power.

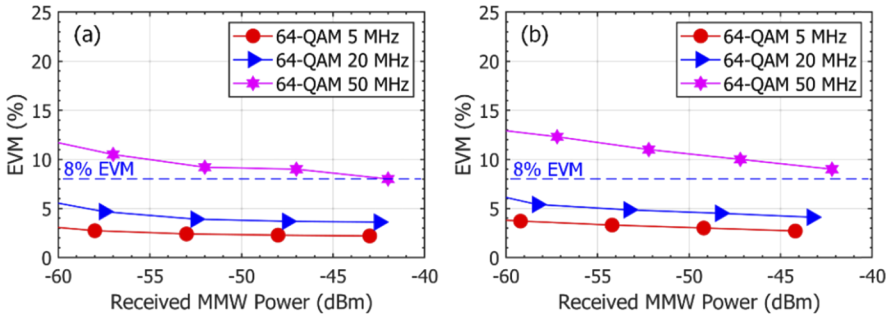

Fig. 3. EVM versus received MMW power of Configuration A with 5 km SSMF, 2 m FSO and 3 m RF wireless for 5, 20 and 50 MHz 64-QAM signals a) without and b) with atmospheric turbulence.

As can be observed, 64-QAM signals with 5 and 20 MHz bandwidth lead to EVM values well below the required limit of 8% regardless of the turbulence level. However, the signal with a 50 MHz bandwidth is more susceptible to turbulence. The impairment due to turbulence-induced fading is then clearly recognized in Fig. 3(b) with the EVMs exceed the 8% required limit at all received MMW powers. This is because of the fact that the wider QAM signal bandwidth, the higher noise power. In addition, 64-QAM signals with 5 and 20 MHz bandwidth were adopted as long-term evolution (LTE) evolved universal terrestrial radio access (E-UTRA) test model TM3.1, which provide a throughput of 18 and 75 Mb/s respectively. Lower data rate signals are less affected by the turbulence-induced intersymbol interference in comparison to 50 MHz 64-QAM signal, which was a custom digital modulation whose bit rate is up to 300 Mb/s. Table 3 summarizes the measured EVMs and calculated BER values for 64-QAM with 5, 20 and 50 MHz 64-QAM without and with turbulence for the hybrid MPL in configuration A at its maximal received MMW power. The turbulence-induced EVM penalties are 0.5, 0.5 and 1% for 5, 20 and 50 MHz, respectively, compared to non-turbulent performances. As can be seen, the EVM

Optics EXPRESS

penalties are relatively small; this is because the generated turbulence is moderate turbulence. However, for strong turbulence (i.e., C_n^2 of 2.4×10^{-10} $m^{-2/3}$ as in [13]), the EVM penalty was about 4% compared with no turbulence. We also evaluate the calculated BER of the M-QAM hybrid MPL based on the EVM as given by [1,3]:

$$\mathrm{BER}_{M-\mathrm{QAM}} = \frac{2}{\log_2(M)}\left(1-\frac{1}{\sqrt{M}}\right)\times \mathrm{erfc}\left(\sqrt{\frac{3}{2(M-1)}\times\frac{1}{\mathrm{EVM}^2}}\right), \tag{4}$$

where erfc(·) is the complementary error function. As shown in Table 3, the BER values are below the HD-FEC BER limit in all cases.

Table 3. Measured EVM and calculated BER results for hybrid MPL (Configuration A) consisting of 5 km SSMF, 2 m FSO and 3 m RF wireless channels.

	Hybrid MPL Performance			
	Without Turbulence		With Turbulence	
64-QAMSignal Bandwidth (MHz)	EVM (%)	BER	EVM (%)	BER
5	2.2	$< 1\times10^{-12}$	2.7	$< 1\times10^{-12}$
20	3.6	3.9×10^{-10}	4.1	2.9×10^{-8}
50	8.0	1.9×10^{-3}	9.0	9.0×10^{-2}

One of the most limiting factors in MPLs is the nonlinear distortion reducing dynamic range and affecting the overall system performance. The link performance was therefore further quantified in terms of 2nd and 3rd nonlinear distortions from which the spurious-free dynamic range (SFDR2 and SFDR3) values have been obtained. Note that the SFDR2 and SFDR3 measurements were carried out by introducing the fundamental signal, i.e., single carriers at frequencies of 200 and 201 MHz to MZM 2 while MZM 1 was fed by 12.5 GHz RF carrier frequency resulting in two tones test at the frequency of 25.2 GHz having 1 MHz spacing. The remaining experimental setup for SFDR measurement was maintained the same as depicted in Fig. 1 including both optical and RF channels to show real system parameters.

Figure 4 shows the measured RF output power as a function of the RF input power $P_{\mathrm{in-RF}}$ for the fundamental frequency and intermodulation distortions (IMDs) (i.e., 2nd and 3rd) components for the hybrid MPL. The overall IMDs refer to the distortions due to nonlinear characteristics of the components employed in the MPL, i.e., EAs. The fitted lines of the 2nd and 3rd order distortions cross the fundamental line at output intercept points (OIP2 and OIP3) with output

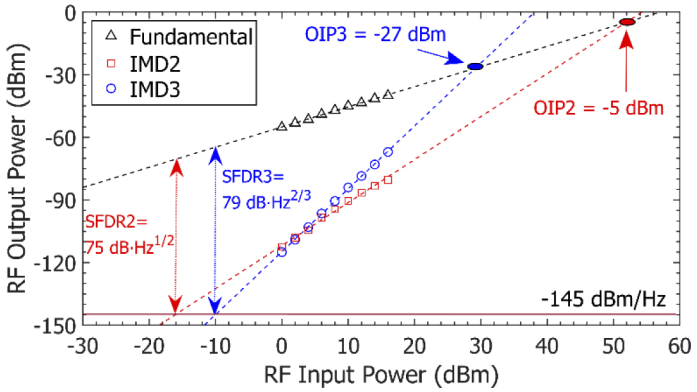

Fig. 4. The measured spurious-free dynamic range of Configuration A.

Optics EXPRESS

power values of -5 and -27 dBm, respectively. The SFDRs are limited by the system noise mainly by the amplifiers such as EAs and EDFA (i.e., amplified spontaneous emission noise). For the proposed system, the measured noise floor is about -145 dBm/Hz, which includes noise contributions from both EA1 and EA2. The resultant SFDR2 and SFDR3 are 75 dB·Hz$^{1/2}$ and 79 dB·Hz$^{2/3}$, respectively. Since we used a broadband signal, the crucial performance parameter is in particular SFDR3. The measured OIP3 and SFDR values are sufficient for the proposed hybrid MPL employing a direct detection receiver. In addition, these can be further improved by adopting a coherent detector [24] or a self-homodyne detector [25] but at the cost of increased complexity. Moreover, the phase noise of the generated signal was determined as low as -107 dBc/Hz at 10 kHz offset.

3.2. Configuration B

To investigate the overall transmission performance of the hybrid MPL for configuration B, which consists of 5 km SSMF and 40 m FSO/RF wireless channels, we first measured the EVM values as a function of the electrical signal-to-noise ratio (SNR) for *M*-QAM signal with 20 MHz bandwidth as shown in Fig. 5. Note that, 20 MHz 4/16/64-QAM signals used were E-UTRA test models TM3.3, 3.2 and 3.1, respectively [23]. For the SNR measurement of each QAM signal at the output of the hybrid MPL, we first adjusted the VOA and then measured the corresponding received MMW power and the noise floor level.

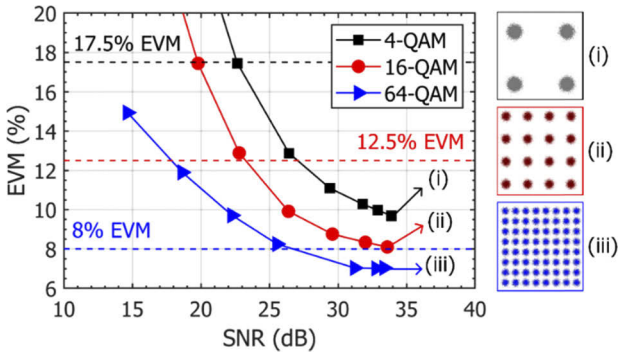

Fig. 5. EVM performance at different SNR levels for 4/16/64-QAM signals with 20 MHz bandwidth of Configuration B with 5 km SSMF, 40 m FSO and 40 m RF wireless links. Insets show corresponding constellations.

The EVM limits of 17.5, 12.5 and 8% for 4-, 16- and 64-QAM, respectively, as defined in the 3GPP specifications [23], are presented by horizontal dashed lines. As shown, at a SNR higher than 27 dB, all *M*-QAM signals meet the EVM requirements. The minimal SNR required to fulfill the limit is 23 dB at an EVM of 12.5% for 16-QAM. The lowest observed EVM values for 4/16/64-QAM are 9.6, 8.1 and 7%, respectively, corresponding to calculated BERs lower than 1×10^{-12}, 1.3×10^{-8} and 5.3×10^{-4}, respectively. All BER values are well below the HD-FEC limit. Also shown in the insets are the clear square-shaped constellations diagrams for *M*-QAM, further demonstrating high-quality signal transmission.

Figure 6 shows the EVM as a function of the received MMW power for *M*-QAM formats with fiber lengths of 5 and 50 km SSMF. Note that, transmission over a 50 km of SSMF (i.e., the maximal expected span for the hybrid MPL in rural areas) is possible due to the OCS modulation scheme effectively combating the fiber chromatic dispersion. As shown in Fig. 6, 4/16/64-QAM meet the EVM requirements for the received minimal MMW power of -49, -48 and -43 dBm, respectively. Moreover, the power penalty for the hybrid link with a 50 km of SSMF compared with 5 km of SSMF is lower than 1 dB for 4- and 16- QAM and 6 dB for 64-QAM. The insets in

Optics EXPRESS

Fig. 6 illustrate discernible constellation diagrams for *M*-QAM for the hybrid MPL with a 50 km of SSMF. Table 4 summarizes the measured EVM and calculated BER values for all three tested signals at its maximal received MMW power. The achieved BER performances for all QAM signals are below the HD-FEC limit.

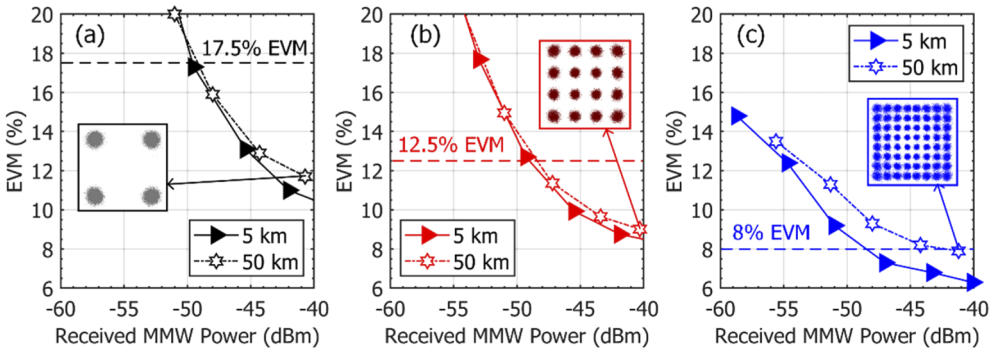

Fig. 6. EVM versus the received MMW power of Configuration B with SSMF lengths of 5 and 50 km, FSO and RF wireless lengths of 40 m: (a) 4-QAM, (b) 16-QAM and (c) 64-QAM format. Insets are the corresponding constellation diagrams.

Table 4. Measured EVM and calculated BER results for hybrid MPL (Configuration B) consisting of 50 km SSMF, 40 m FSO and 40 m RF wireless.

	Hybrid MPL Performance	
M-QAM (20 MHz)	EVM (%)	BER
4-QAM	11.7	$< 1\times10^{-12}$
16-QAM	9.0	2.5×10^{-7}
64-QAM	7.9	1.7×10^{-3}

Furthermore, we examined the effect of multipath-induced fading in the hybrid MPL with 20 MHz 64-QAM at 25 GHz by measuring the EVM as a function of the Rx ANT's angular orientation (also known as ANT misalignment) utilizing a high-precision rotation mount. The results are shown in Fig. 7. Note that, for ANT misalignment measurements, the hybrid MPL was composed of 50 km SSMF, 40 m FSO and 40 m RF wireless links. We observed EVM

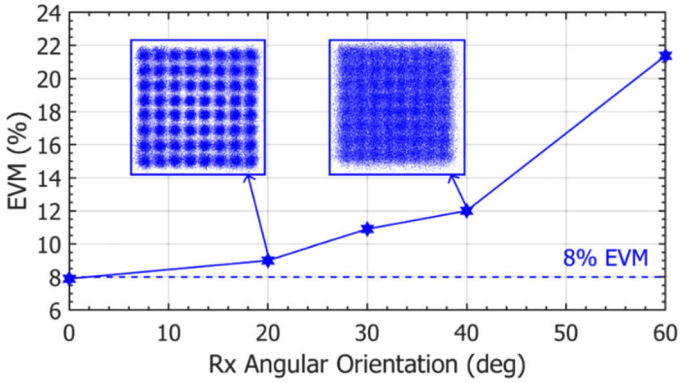

Fig. 7. EVM performance of the 64-QAM signal (Configuration B) under the variable angular orientation of Rx ANT off-axis of propagation.

Optics EXPRESS

impairment (i.e., above the limit of 8%) at the angular orientation values > 3°. This is because of fading due to reflected signals from walls along the 40 m corridor and the first Fresnel zone, which affects the signal strength. To better illustrate the impact of fading, the insets in Fig. 7 shows the measured constellation diagrams at the angular orientation values of 20° and 40°, which are distorted but still identifiable even for the EVMs significantly higher than 8% limit. However, the degradation of EVM/BER performance due to the RF wireless channel effects can be overcome by means of modulation, coding and adaptive equalization schemes [26,27]. Recently, the ANT misalignment has also been investigated in the D-band (141 GHz) RoF system, but over short RF wireless length of only 0.5 m [28], where the tolerable misalignment angle was found to be less than 1°. Note that, as reported in [28], angles higher than 1° lead to the increased BER above the HD-FEC limit.

4. Evaluation for extended outdoor link length

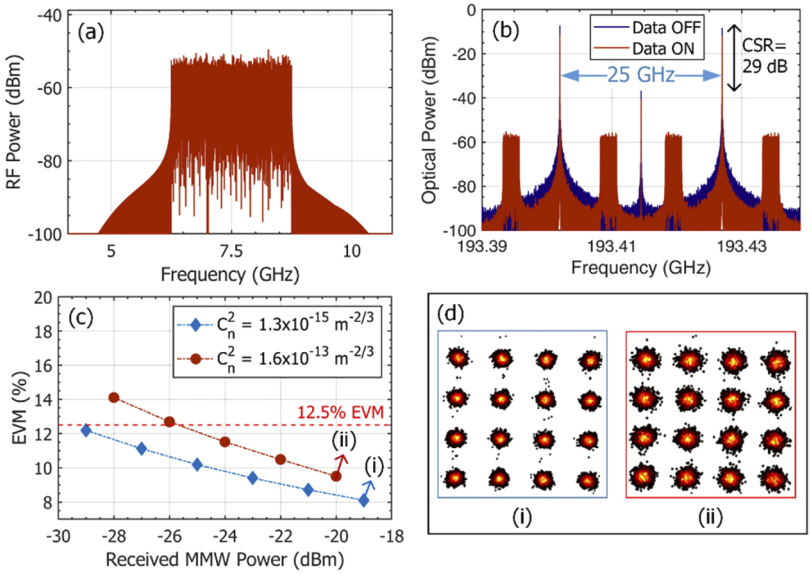

Fig. 8. Simulation results for hybrid MPL of 5 km SSMF and 500 m FSO links: (a) Electrical spectrum of transmitted 16-QAM signal, (b) Optical spectra obtained without and with 16-QAM data signal (c) EVM versus received MMW power for 10 Gb/s 16-QAM under weak and strong turbulence and (d) Corresponding constellation diagrams.

To further evaluate the proposed hybrid MPL for a practical outdoor scenario as part of the 5G network, we performed a simulation-based analysis at a bit rate of 10 Gb/s and a carrier frequency of 25 GHz using OptiSystem and MATLAB software co-simulation [29]. In detail, OptiSystem is used to accurately model the hybrid MPL as the experimental setup while MATLAB is used for signal analysis, i.e., EVM calculation. The link is composed of a 5 km of SSMF, however the FSO length is extended up to 500 m. The RF wireless link is not considered in this investigation. We have considered the weak and strong turbulence regimes in FSO channel with C_n^2 of 1.3×10^{-15} $m^{-2/3}$ and 1.6×10^{-13} $m^{-2/3}$, respectively. The simulation parameters are the same as those employed in Configuration B. A 16-QAM-based OFDM over IF of 7.5 GHz with a total signal bandwidth of 2.5 GHz was transmitted, as shown in Fig. 8(a). Figure 8(b) shows the simulated OCS spectrum with and without the 10 Gb/s 16-QAM signal. The CSR is about 29 dB demonstrating a good agreement between simulation and experimental results as can be seen in the inset (iv) in Fig. 1. Figure 8(c) illustrates the simulated EVM as a function of the received

Optics EXPRESS

MMW power for 16-QAM under the weak and strong turbulence conditions in the FSO channel. As shown, 16-QAM meets the EVM requirement of 12.5% at the received MMW power level > -25.5 dBm. For weak and strong turbulence regimes, the lowest obtained EVM values are 8.1 and 9.5%, which correspond to the BER values of 1.3×10^{-8} and 9.4×10^{-7}, respectively. It is worth mentioning that, there is a distinctive difference of > 20 dB between the experimentally measured (see Fig. 3) and simulated (see Fig. 8(c)) power levels. This is because, the simulated results are for the 10 Gb/s hybrid link requiring more power whereas the measured data is for the 300 Mb/s link (i.e., 50 MHz 64-QAM).

The effect of turbulence on the link performance can also be comprehended by means of the constellation diagrams, see Fig. 8(d), which are still distinguishable even under strong turbulence, thus confirming the feasibility of the proposed hybrid scheme for practical applications. Note that, the power penalty due to turbulence can be reduced by using a digital turbulence compensation technique which is a combination of a 12-spatial mode digital coherent receiver and a multimode pre-amplifier as recently demonstrated in [30].

5. Conclusions

We have proposed and experimentally demonstrated a hybrid microwave photonic link at the K-band having the frequency of 25 GHz with two different configurations. We demonstrated potential applications in seamless broadband wireless access networks. For the first configuration, we examined the hybrid MPL consisting of 5 km SSMF, 2 m turbulent FSO and 3 m RF wireless channels with the focus on the effect of turbulence-induced fading on the 64-QAM signals with 5, 20 and 50 MHz bandwidths. We determined the non-linear distortions by showing that the 2nd and 3rd order SFDRs of the hybrid MPL are 75 and 79 dB·Hz$^{2/3}$, respectively, as well as overall phase noise below -107.3 dBc/Hz at 10 kHz offset. For the second MPL configuration, we individually transmitted 20 MHz 4/16/64-QAM signals over 50 km of SSMF, 40 m FSO and 40 m RF wireless channels and compared the performance. Depending on the data rates and applications, each modulation can be adaptively configured. The result showed that the recovered signals displayed EVM values well below the required limits as defined by 3GPP specifications with no significant received MMW power penalties. The tolerable ANT misalignment angle for such an indoor corridor transmission was also investigated and found to be less than 3°. Moreover, we have provided a simulation analysis carried out for 10 Gb/s 16-QAM link with the FSO span of 500 m under weak and strong turbulence conditions in the FSO channel. The experimental and simulation results have demonstrated the feasibility of the proposed hybrid MPL for use in practical applications since the scheme reduces demands on high-frequency equipment and therefore showing high potential for the 5G wireless networks.

Funding

The Ministry of Education, Youth and Sports of Czech Republic (CZ.02.2.69/0.0/0.0/16_027/0008465); Czech Technical University in Prague (SGS17/182/OHK3/3T/13).

References

1. X. Chen and J. Yao, "A high spectral efficiency coherent microwave photonic link employing both amplitude and phase," J. Lightwave Technol. **33**(14), 3091–3097 (2015).
2. Y. Li, Q. Yang, I. A. Hemadeh, M. El-Hajjar, C.-K. Chan, and L. Hanzo, "Experimental characterization of the radio over fiber aided twin-antenna spatial modulation downlink," Opt. Express **26**(10), 12432 (2018).
3. W. Zhang, A. Wen, Y. Li, and J. Ma, "A high spectral efficiency microwave photonic link with optimization of chromatic-dispersion-induced power fading," J. Lightwave Technol. **37**(4), 1123–1132 (2019).
4. L. Zhang, M. Zhu, C. Ye, S.-H. Fan, C. Liu, X. Hu, P. Cao, Q. Chang, Y. Su, and G.-K. Chang, "Generation and transmission of multiband and multi-gigabit 60-GHz MMW signals in an RoF system with frequency quintupling technique," Opt. Express **21**(8), 9899 (2013).
5. S. E. Alavi, M. R. K. Soltanian, I. S. Amiri, M. Khalily, A. S. M. Supa'at, and H. Ahmad, "Towards 5G: A photonic based millimeter wave signal generation for applying in 5G access fronthaul," Sci. Rep. **6**(1), 19891 (2016).

Optics EXPRESS

6. H. Wen, H. Zheng, Q. Mo, A. M. Velázquez-Benítez, C. Xia, B. Huang, H. Liu, H. Yu, P. Sillard, J. E. A. Lopez, R. A. Correa, and G. Li, "Few-mode fibre-optic microwave photonic links," Light: Sci. Appl. **6**(8), e17021 (2017).
7. C. Vagionas, S. Papaioannou, G. Kalfas, N. Pleros, N. Argyris, K. Kanta, N. Iliadis, G. Giannoulis, D. Apostolopoulos, and H. Avramopoulos, "A six-channel mmWave/IFoF link with 24Gb/s capacity for 5G fronthaul networks," in *MWP 2018 – 2018 International Topical Meeting on Microwave Photonics* (IEEE, 2018), p. Tu4B.6.
8. Z. Ghassemlooy, W. O. Popoola, and S. Rajbhandari, *Optical Wireless Communications – System and Channel Modelling with Matlab*, 2nd ed. (CRC Press, 2019).
9. K. Wang, A. Nirmalathas, C. Lim, K. Alameh, and E. Skafidas, "Full-duplex gigabit indoor optical wireless communication system with CAP modulation," IEEE Photonics Technol. Lett. **28**(7), 790–793 (2016).
10. K. Kazaura, K. Wakamori, M. Matsumoto, T. Higashino, K. Tsukamoto, and S. Komaki, "RoFSO: A universal platform for convergence of fiber and free-space optical communication networks," IEEE Commun. Mag. **48**(2), 130–137 (2010).
11. C. Ben Naila, K. Wakamori, M. Matsumoto, A. Bekkali, and K. Tsukamoto, "Transmission analysis of digital TV signals over a radio-on-FSO channel," IEEE Commun. Mag. **50**(8), 137–144 (2012).
12. J. Zhang, J. Wang, Y. Xu, M. Xu, F. Lu, L. Cheng, J. Yu, and G.-K. Chang, "Fiber–wireless integrated mobile backhaul network based on a hybrid millimeter-wave and free-space-optics architecture with an adaptive diversity combining technique," Opt. Lett. **41**(9), 1909 (2016).
13. J. Bohata, M. Komanec, J. Spáčil, Z. Ghassemlooy, S. Zvánovec, and R. Slavík, "24–26 GHz radio-over-fiber and free-space optics for fifth-generation systems," Opt. Lett. **43**(5), 1035–1038 (2018).
14. M. A. Esmail, A. M. Ragheb, H. A. Fathallah, M. Altamimi, and S. A. Alshebeili, "5G-28 GHz signal transmission over hybrid all-optical FSO/RF link in dusty weather conditions," IEEE Access **7**, 24404–24410 (2019).
15. R. M. Borges, T. R. R. Marins, M. S. B. Cunha, H. R. D. Filgueiras, I. F. Da Costa, R. N. Da Silva, D. H. Spadoti, L. L. Mendes, and A. C. Sodre, "Integration of a GFDM-based 5G transceiver in a GPON using radio over fiber technology," J. Lightwave Technol. **36**(19), 4468–4477 (2018).
16. "5G spectrum GSMA public policy position," https://www.gsma.com/.
17. R. Zhang, F. Lu, M. Xu, S. Liu, P. Peng, S. Shen, J. He, H. J. Cho, and Q. Zhou, "An ultra-reliable MMW / FSO A-RoF system based on coordinated mapping and combining technique for 5G and beyond mobile fronthaul," J. Lightwave Technol. **36**(20), 4952–4959 (2018).
18. A. Pandey and S. K. Selvaraja, "Broadly tunable wideband optical single sideband generation using self-coupled silicon resonator," Opt. Express **27**(6), 8476 (2019).
19. P. T. Dat, A. Kanno, and N. Yamamoto, "Seamless convergence of fiber and wireless systems for 5G and beyond networks," J. Lightwave Technol. **37**(2), 592–605 (2019).
20. M. A. Esmail, A. Ragheb, H. Fathallah, and S. Alshebeili, "Demonstration of photonics-based switching of 5G signal over hybrid all-optical network," IEEE Photonics Technol. Lett. **30**(13), 1250–1253 (2018).
21. Y. Alfadhli, P. C. Peng, H. Cho, S. Liu, R. Zhang, Y. W. Chen, and G. K. Chang, "Real-time FPGA demonstration of hybrid bi-directional MMW and FSO fronthaul architecture," in *2019 Optical Fiber Communications Conference and Exhibition, OFC 2019 – Proceedings* (OSA, 2019), p. W2A.39.
22. L. C. Andrews and R. L. Phillips, *Laser Beam Propagation through Random Media* (SPIE, 2005), 1.
23. 3GPP TS 36.104, *Base Station (BS) Radio Transmission and Reception (2018)*, **version 16**(version 16.0.0).
24. R. Li, X. Han, X. Chen, X. Chen, and J. Yao, "A phase-modulated microwave photonic link with an extended transmission distance," IEEE Photonics Technol. Lett. **27**(24), 2563–2566 (2015).
25. P. T. Dat, A. Kanno, N. Yamamoto, and T. Kawanishi, "Full-duplex transmission of LTE-A carrier aggregation signal over a bidirectional seamless fiber-millimeter-wave system," J. Lightwave Technol. **34**(2), 691–700 (2016).
26. J. Proakis and M. Salehi, *Digital Communications*, 5th ed. (McGraw-Hill, 2008).
27. T. F. B. de Sousa and M. A. C. Fernandes, "Butterfly neural equalizer applied to optical communication systems with two-dimensional digital modulation," Opt. Express **26**(23), 30837 (2018).
28. R. Puerta, J. Yu, X. Li, Y. Xu, J. J. Vegas Olmos, and I. Tafur Monroy, "Antenna misalignment effects in 100 Gbit/s D-band wireless transmissions," Microw. Opt. Technol. Lett. **59**(6), 1431–1434 (2017).
29. "OptiSystem archives-Optiwave," https://optiwave.com/.
30. N. K. Fontaine, R. Ryf, Y. Zhang, J. C. Alvarado-Zacarias, S. Van Der Heide, M. Mazur, H. Huang, H. Chen, R. Amezcua-Correa, G. Li, M. Capuzzo, R. Kopf, A. Tate, H. Safar, C. Bolle, D. T. Neilson, E. Burrows, K. Kim, M. Bigot-Astruc, F. Achten, P. Sillard, A. Amezcua-Correa, and J. Carpenter, "Digital turbulence compensation of free space optical link with multimode optical amplifier," in *European Conference on Optical Communication, ECOC 2019*, p. PD1.1.